Journal of Hazardous Materials 190 (2011) 268–275

Contents lists available at ScienceDirect

Journal of Hazardous Materials

journal homepage: www.elsevier.com/locate/jhazmat

Validation of a numerical code for the simulation of a short-term CO_2 release in an open environment: Effect of wind conditions and obstacles

E. Papanikolaou, M. Heitsch, D. Baraldi*

European Commission DG-JRC, Institute for Energy–Cleaner Energy Unit 1755 ZG, Petten, The Netherlands

ARTICLE INFO

Article history:
Received 23 November 2010
Received in revised form 11 March 2011
Accepted 11 March 2011
Available online 21 March 2011

Keywords:
CFD validation
CCS
CO_2
Safety
Gas release

ABSTRACT

Carbon Capture and Storage (CCS) is one of the possible mitigation measures to reduce the CO_2 emissions produced from anthropogenic sources and thus help address the issue of global warming. Accidental CO_2 releases may occur at any of the CCS stages, having potentially harmful consequences on the people who work in the CCS facilities, the general public in their vicinity and the environment.

CFD is an increasingly used tool to investigate the behavior of released substances and predict the consequences of hazardous scenarios. This information aids the development of mitigation methods to minimize the consequences of an accident. The validation of numerical codes and models is a necessary preliminary step before their application to safety and risk assessment analysis. In this context, numerical simulations of CO_2 release and dispersion field experiments were performed with a CFD code. The experimental data were taken from the Kit Fox CO_2 gas field experiments which were designed to investigate the effect of ground roughness of industrial process plants and of meteorological conditions on the formation and extent of the CO_2 gas cloud. This study presents a comparison between the simulation results and the experimental measurements in order to assess the accuracy of the code with different modeling approaches.

1. Introduction

Carbon Capture and Storage (CCS) technologies seek to capture the CO_2 that would otherwise be emitted from large combustion plants (primarily fossil fuel power stations, cement and steel plants) and store it for a long period of time and thus help address the issue of global warming. CCS is an integrated process involving: capturing CO_2 from plants, separation from other gaseous products, compression at the capture facility, transportation and storage through injection into geological structures. Accidental CO_2 releases may occur at any of the aforementioned stages of the overall process and may pose a threat to humans and environment.

The ability to anticipate foreseeable accidental scenarios and predict their consequences is a fundamental element in the assessment of the risk of a process or technology. The difficulties in identifying accurately the hazards associated with a novel process or technology, such as CCS, mainly originate from the limited operation experience. However, in the USA there are currently 74 projects in which 33 million tones of CO_2 are injected annually into oil fields for Enhanced Oil Recovery (EOR). A more limited amount of CO_2 is used for EOR projects in other countries. The IEA roadmap on CCS identifies a detailed scenario for the technology growth from a handful of current large-scale projects to over three thousand projects by 2050 [1]. The European Strategic Energy Technology Plan (SET-Plan) [2] identifies the objective of demonstrating the commercial viability of CCS technologies in an economic environment driven by the emissions trading scheme, and in particular, to enable their cost competitive deployment in coal-fired power plants by 2020 or soon after. The European Commission established a strategy to support the development of CCS projects, including the launch of a European Industrial Initiative on CCS [3] and the co-financing of six large-scale projects through the European Energy Programme for Recovery (EEPR) within the frame of the European Economic Recovery Plan (EERP). Another EU financing instrument for CCS projects is the New Entrants Reserve (NER300) of the European Emissions Trading Scheme. The European Commission initiated also the world's first network of demonstration projects (The European CCS Demonstration Project Network), to encourage and facilitate knowledge sharing among the CCS projects with the final goal of achieving commercially viable CCS by 2020.

If CCS technology is to be commercialized widely, safety issues concerning all the stages of this technology should be addressed. These issues have been mentioned several times in the European Directive on the geological storage of CO_2 [4]. Exposure to CO_2 can potentially lead to coma and even death, depending on the concentration and exposure time. The CO_2 Workplace Exposure Limits in

* Corresponding author. Tel.: +31 (0)224 565140; fax: +31 (0)224 5630.
E-mail address: daniele.baraldi@jrc.nl (D. Baraldi).

0304-3894/$ – see front matter © 2011 Elsevier B.V. All rights reserved.
doi:10.1016/j.jhazmat.2011.03.041

Nomenclature

C_o	CO_2 observed concentration (molar fraction)
C_p	CO_2 predicted concentration (molar fraction)
$\overline{C}$	average concentration over the dataset
c_p	specific heat capacity of dry air (1020 J/kg K)
g	acceleration of gravity (=9.81 m/s^2)
k	turbulence kinetic energy (m^2/s^2)
L	Monin-Obukhov length scale (m)
T	temperature (K)
T_w	ground temperature (K)
T_*	dynamical temperature (K)
u	velocity (m/s)
u_*	friction velocity (m/s)
z	height (m)
z_0	roughness height (m)

Greek letters

ε	turbulence dissipation rate (m^2/s^3)
κ	von Karman constant (=0.4)

the UK are: 0.5% (5000 ppm) for the 8 h Long Term Exposure Limit and 1.5% (15,000 ppm) for the 15 min Short Term Exposure Limit [5]. The exposure threshold at which CO_2 is immediately dangerous to human life or health is 70,000–100,000 ppm [6]. The largest disaster in terms of fatalities due to accidental CO_2 release was a natural event. In 1986 a large cloud of CO_2 was released from the CO_2 saturated water of Lake Nyos in Cameroon due to a landslide, killing 1700 people and 3500 livestock in nearby villages.

Numerical codes and models are increasingly used tools to investigate the behavior of a released substance and predict the consequences of a hypothetical hazardous scenario. This information aids the development of mitigation methods to minimize the consequences of an accident. Validation of numerical codes and models is a necessary preliminary step before the application of the models/codes to safety and risk assessment analysis. In this context, this work presents numerical simulations of a CO_2 release and dispersion field experiment with the CFD code ANSYS CFX 12.1 [7]. A systematic comparison between the simulation results and the experimental measurements is presented in order to assess the accuracy of the numerical code and of the modeling approaches. The experimental data were taken from the Kit Fox CO_2 gas field experiments which covered ground level short-duration transient and continuous releases [8].

Previous numerical investigations aiming at the validation of codes and models for gas field experiments include the work performed by Hanna and Chang [9], Hanna et al. [10], and Mazzoldi et al. [11]. A clear indication from those previous numerical studies is that the modeling of the obstacles and of the wind conditions are influential parameters on the predicted gas concentrations. Therefore, in this study it was decided to investigate both these parameters and evaluate their impact on the simulation results.

2. Description of the Kit Fox experiments

The Kit Fox experiments were carried out in the summer of 1995 at the US Department of Energy (DOE) Nevada test site which is a flat dry lake bed in the middle of the desert [8]. The experiments were designed to investigate the effect of ground roughness of industrial process plants and of meteorological conditions on the formation and extent of the gas cloud caused by short and continuous releases. Constructing a full scale mock-up of a typical refinery or industrial plant was found impractical so the experimental field was scaled down to 1:10. Two types of obstacle arrays were used to represent the roughness typical of such a site; namely the URA (Uniform Roughness Array) or large obstacles and ERP (Enhanced Roughness Pattern) or small obstacles. The small obstacles were approximately, 6600 and were distributed in 133 arrays. The large obstacles were 75 and were distributed in 11 arrays. Both types of obstacles were flat baffles facing the prevailing wind direction with dimensions of 0.8 m width and 0.2 m height (URA obstacles) and 2.4 m width and 2.4 m height (ERP obstacles). To avoid channeling of the flow along the baffle rows, the obstacles were staggered from one row to the other. Additionally, 36 spires with 4.9 m height were located just before the ERP and URA obstacles in order to decrease the distance required for the boundary layer development.

The 1.5 m by 1.5 m CO_2 release area was located in the middle of the width of the arrays and 89 m from the beginning of the URA (shown in Fig. 1). Concentration measurements were recorded by 84 sensors in 4 arrays located at 25 (array 1), 50 (array 2), 100 (array 3) and 225 m (array 4) downwind of the CO_2 release. Meteorological measurements were made on towers inside and outside the obstacle arrays. A full description of the experiments and data processing can be found in [8].

The experimental test selected for validation of the CFD code was a short-term (20 s) CO_2 release. The details of the experimental conditions of the test are shown in Table 1. The maximum reported CO_2 concentration was 8500 ppm at the sensor closest to the release area.

3. Description of the simulations set-up

The numerical work was carried out with ANSYS–CFX version 12.1 [7]. Turbulence was modeled using the standard k-epsilon model. The convective and temporal terms were discretised with 2nd order accurate schemes. Convergence was controlled by setting a target value of the normalized equation residuals equal to

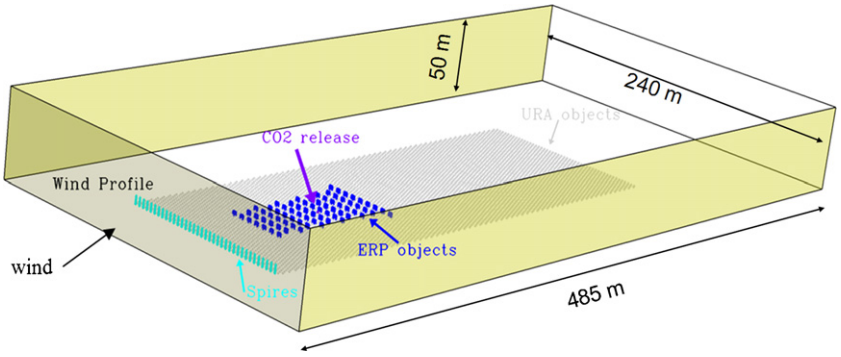

Fig. 1. Layout of the modeled experimental site (with fully resolved URA and ERP obstacles and spires).

Table 1
Experimental conditions of the selected case for CFD validation.

Experimental conditions	
Release duration (s)	20
Release rate (kg/s)	3.65
Total mass released (kg)	73
Release temperature (K)	298
Ambient temperature (K) at 2 m	304
Ground temperature (K)	302
Average wind speed (m/s) at 2 m	1.14
Type of obstacles present	URA and ERP
Pasquil-Gifford stability class	F (stable)
Friction velocity (m/s)	0.21
Roughness length for URA only configuration (m)	0.03
Monin-Obukhov length (m)	17

10^{-4}. The size of the time step was bound with a minimum and maximum of 10^{-4} and 10^{-1} s respectively.

Table 2 shows the cases used for investigating the effect of the modeling approach of the wind conditions and the obstacles on site. In Cases 1, 2 and 3 both URA and ERP obstacles were fully resolved on the computational mesh whereas in Case 4 only the ERP obstacles were fully resolved. In this case the URA obstacles were substituted by a roughness height of 0.03 m as suggested by the experimental description. In Cases 2 and 4 the wind had a constant in time average profile calculated based on the experimental data. In Case 3, the wind profile was kept constant but with double average velocity compared to the one used in Cases 2 and 4 in order to investigate the effect of a different wind velocity on the simulation results. Finally, in Case 1 the wind profile varied in time. The approach used to calculate the temporal variation of the wind is explained in Section 3.2.

3.1. Domain and mesh

The mesh generation was realized with the commercial software Gridgen version 15.15 from Pointwise Inc. [12]. The small-sized URA obstacles were resolved in the computational mesh by using solid faces (baffles) of zero thickness. As can be seen from Fig. 1, the computational domain was extended far from the experimental site to reduce the effect of the boundary conditions on the simulations. The dimensions of the computational domain were 485 m length by 240 m width by 50 m height whereas the experimental facility had 314 m length and 120 m width. The mesh was tetrahedral unstructured. The size of the mesh was 1,900,000 nodes for Case 4 and 2,500,000 nodes for the rest of the cases. Appropriate refinement close to the ground and the obstacles was chosen for all cases.

In order to check grid independence, two simulations were performed with 2 finer grids for Case 4. Given the prohibitively long computer run-time, it was possible to investigate grid independence only for Case 4 and only for a region of the computational domain. The approach of investigating the grid independence only in a region instead than in the whole computational domain for cases that require high computational resources was presented by several authors including Blazek [22] and Ferziger and Peric [23]. The grid refinement was performed in the region close to the ground where both the obstacles and the sensors are located and where a higher resolution might be required in order to achieve a better accuracy. In the 1st refined mesh, the number of nodes was doubled in the selected region as compared to the initial simulation. Originally the region contained 1,000,080 nodes while the whole mesh consisted of 1,899,000 nodes. The refinement resulted in 1,000,080 additional nodes in the selected region. The 2nd refined grid was generated by further refining the computational mesh and this refinement produced 2,715,000 additional nodes compared to the initial simulation. A comparison between the results of the successive refinements was carried out, sensor by sensor and the averaged difference of the results (maximum CO_2 concentration in the sensors) between the original coarser grid and the two refined grids is about 3%.

Table 2
Simulation cases.

Case	Wind profile	Obstacles on computational mesh
1	Variable in time	URA and ERP
2	Constant in time	URA and ERP
3	Constant in time with double average velocity	URA and ERP
4	Constant in time	ERP

3.2. Boundary and initial conditions

A no-slip condition was applied on the ground using the default wall functions of the code. An outlet boundary condition was applied at the plane opposite the wind inlet. A symmetry boundary condition was set to the lateral planes and a slip boundary condition was assigned at the top plane as suggested in [13]. An inlet boundary condition was set at the CO_2 release source based on the experimental description (Table 1).

An inlet boundary condition was assigned to the plane located at the prevailing wind direction (see Fig. 1) where the variables assumed either a constant in time profile (Cases 2, 3 and 4) or a specified varying in time profile (Case 1). A description of the profiles is given below.

The conditions of the wind velocity, temperature, turbulence and its dissipation for the inlet wind plane were calculated using the Monin–Obukhov similarity theory as described in [14,15] (a description of the symbols is given in the nomenclature):

$$u(z) = \frac{u_*}{\kappa}\left[\ln\left(\frac{z}{z_0}\right) + \Phi_m\left(\frac{z}{L}\right) - 1\right] \quad (1)$$

$$T(z) = T_w + \frac{T_*}{\kappa}\left[\ln\left(\frac{z}{z_0}\right) + \Phi_m\left(\frac{z}{L}\right) - 1\right] - \frac{g}{c_p}(z - z_0) \quad (2)$$

$$k(z) = \frac{u_*^2}{\sqrt{C_\mu}}\sqrt{\frac{\Phi_h\left(z/L\right)}{\Phi_m\left(z/L\right)}} \quad (3)$$

$$\varepsilon(z) = \frac{u_*^3}{z\kappa}\Phi_h\left(\frac{z}{L}\right) \quad (4)$$

$$T_* = \frac{u_*^2 T_w}{gL\kappa} \quad (5)$$

$$u_* = \sqrt{\frac{\tau_w}{\rho}} \quad (6)$$

where $C_\mu = 0.09$, $\kappa = 0.4$ and for stable atmospheric conditions the functions Φ_m and Φ_h have the following form:

$$\Phi_m\left(\frac{z}{L}\right) = 1 + 5\frac{z}{L}, \quad \text{for } \frac{z}{L} \geq 0 \quad (7)$$

$$\Phi_h\left(\frac{z}{L}\right) = 1 + 4\frac{z}{L}, \quad \text{for } \frac{z}{L} \geq 0 \quad (8)$$

The variation of the friction velocity and dynamical temperature (u_* and T_*) with time was calculated using the experimental values of u and T at the available monitoring points using Eqs. (1) and (2). The profile over time of these 2 quantities that resulted in the best fit of u and T at the monitoring points was selected as input for Eqs. (1)–(4) which in turn were used as boundary conditions at the inlet wind plane. Figs. 2 and 3 show the resulting velocity profile at the wind inlet plane at 2 m height over time and at 10 s over height

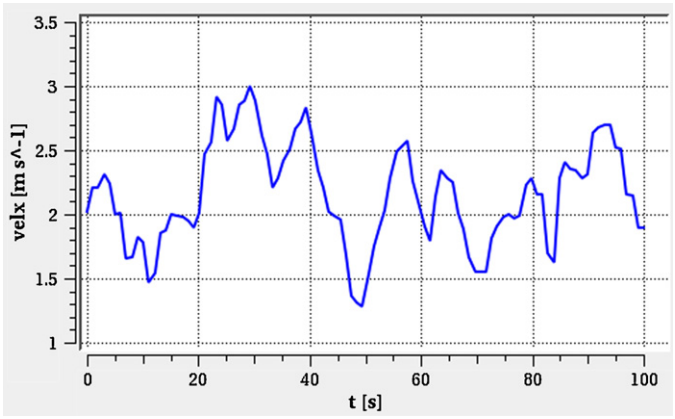

Fig. 2. Temporal variation of velocity at 2 m height of the wind inlet plane.

respectively. For the cases with constant wind profile, the friction velocity and dynamical temperature were assigned a constant value as suggested in the report of the experimental description [8]. It should be noted that for the specific experimental test the variation of the direction of the wind was not significant enough to be modeled. Therefore, in all cases the wind direction was assumed constant and as shown in Fig. 1.

The initial conditions of the wind field over the computational domain were the same as the boundary conditions at the wind inlet in order to initialize the flow field uniformly.

The CO_2 release started 50 s from the beginning of the simulation in order to allow the wind flow field to develop over the computational domain before releasing the gas. This time was found sufficient to ensure a developed wind flow field. Additionally, for the case with varying wind velocity and temperature profiles, the numerical results were compared with the experimental data at the 4 meteorological masts throughout the simulation time. The agreement was quite satisfactory.

4. Statistical performance indicators

Statistical performance indicators for the ratio of the maximum observed (C_o) and maximum predicted (C_p) CO_2 concentrations at each sensor for each array were used in order to evaluate the performance of the simulated cases in a systematic way. These indicators were recommended by Chang and Hanna [16] for evaluating air dispersion models and a short description of them is given below:Geometric Mean Bias (MG): measures relative mean bias and indicates only systematic errors based on a logarithmic scale.

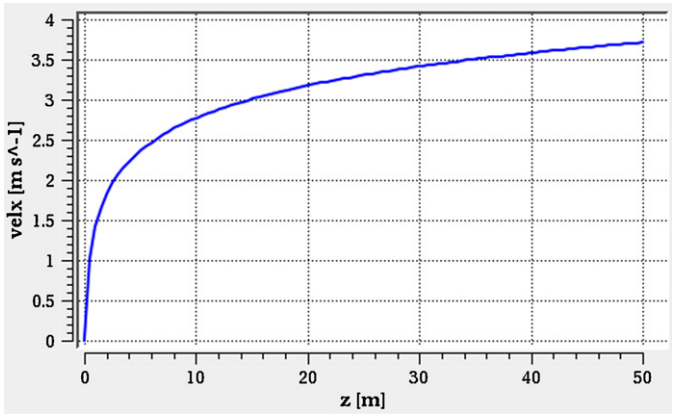

Fig. 3. Velocity profile at 10 s of the wind inlet plane.

Values of 0.5 and 2.0 can be thought of as 'factor of two' over- and under-predictions in the mean, respectively. It has a value of 1 for an ideal model performance.

$$\mathrm{MG} = \exp\ (\overline{\ln C_o} - \overline{\ln C_p}) \tag{9}$$

Geometric Mean Variance (VG): measures relative scatter. It has a value of 1 for an ideal model performance.

$$\mathrm{VG} = \exp\left[\overline{(\ln C_o - \ln C_p)^2}\right] \tag{10}$$

Fraction within a factor of 2 (FAC2): fraction of data that satisfy the following relationship:

$$0.5 \le \frac{C_p}{C_o} \le 2.0 \tag{11}$$

The CO_2 concentration was measured with high (with $0–5 \times 10^{-2}$ m^3/m^3 or $0–15 \times 10^{-2}$ m^3/m^3 measurement range) and low ($0–2 \times 10^{-3}$ m^3/m^3 or $0–2 \times 10^{-2}$ m^3/m^3 measurement range) concentration sensors. During the processing of the results, the reported experimental values that were lower than the accuracy (1% of full range) of the sensors were not taken into account and thus their respective predicted values of all the cases were also excluded (in total 7 sensor readings). For the calculation of MG and VG, Chang and Hanna [16] suggested to set a lower bound for both observed and predicted concentrations because these indicators are highly influenced by extremely low values. The suggestion was followed and the predicted values with concentration below the detection limit were substituted by the detection limit of the respective sensors.

5. Results and discussion

Figs. 4 and 5 show a comparison between the experimental CO_2 concentration readings with the simulation results for the sensors closer to the release area (i.e. 25 m far in the x direction and at the center of the array) at $z = 0.3$ m and $z = 1.2$ m for Case 1 (sensors P1001 and P1003 respectively). The graphs show a good agreement between the simulation and the data. The prediction of the concentration peak is about 15 s earlier than the experimental.

Table 3 shows a summary of the performance of the simulations. For each case the values of the statistical indicators were grouped for each of the 4 arrays separately and for all the sensors (overall performance). The table also shows the maximum volumetric

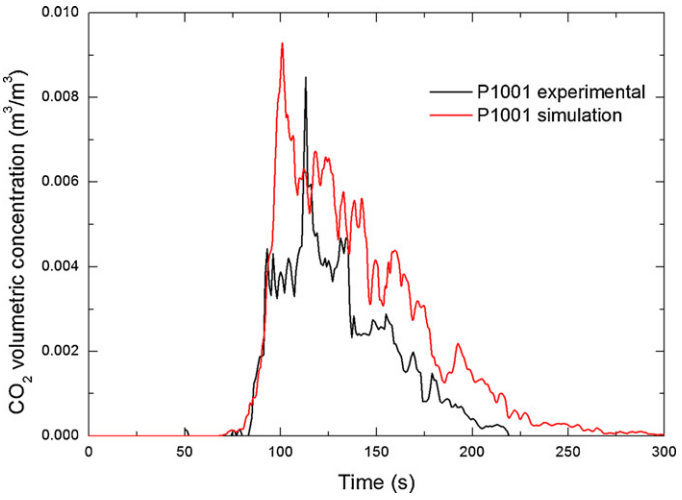

Fig. 4. Comparison of experimental CO_2 concentration readings with simulation at sensor P1001 (release starts at 50 s).

Table 3
Summary of simulations' performance using statistical indicators; the acceptable range is given in the last row. Values outside the acceptable range are highlighted in yellow.

	Array (distance from release in m)	MG	VG	FAC2	C max (v/v/)
Case 1	1 (25)	0.67	1.28	0.85	
	2 (50)	1.11	1.53	0.84	
	3 (100)	1.13	1.49	0.68	
	4 (225)	1.88	2.35	0.57	
	Overall	**1.00**	**1.50**	**0.77**	**0.015**
Case 2	1 (25)	1.14	2.03	0.76	
	2 (50)	1.08	1.66	0.73	
	3 (100)	1.21	2.23	0.78	
	4 (225)	3.03	9.16	0.43	
	Overall	**1.27**	**2.31**	**0.73**	**0.012**
Case 3	1 (25)	1.58	3.04	0.62	
	2 (50)	1.78	3.55	0.37	
	3 (100)	1.78	4.89	0.58	
	4 (225)	3.65	13.67	0.14	
	Overall	**1.84**	**4.27**	**0.48**	**0.014**
Case 4	1 (25)	1.13	2.28	0.62	
	2 (50)	1.09	1.52	0.89	
	3 (100)	1.36	2.20	0.68	
	4 (225)	3.22	7.83	0.28	
	Overall	**1.32**	**2.29**	**0.68**	**0.013**
	Acceptable range and ideal value [16]	0.7<MG<1.3 MG=1	VG<4 VG=1	0.5<FAC2<2 FAC2=1	

concentration C_{max} predicted for all cases. The highest concentration was predicted in Case 1, however the difference with the other cases was only 20%. The overall performance of Case 1 and 2 was within the range of the acceptable criteria as suggested by Chang and Hanna with Case 1 performing better than the rest of the cases for all the criteria examined. For Case 4 MG is just outside the acceptable range (MG = 1.32) while the other two statistical indicators are within that range. FAC2 is the most robust indicator because it is not highly influenced by high and low values. As can be seen from the table, in Case 1 77% of the sensors were within a factor of two of the observations following by Case 2 with 73% and Case 4 with 68%. For Case 3 the MG and VG values were higher than the maximum acceptable while the FAC2 was lower than the minimum acceptable. This case is the same as Case 2 but with a double average velocity than the average experimental value and therefore it was expected to perform the worst. For all cases FAC2 had the lowest value in the array 4 as compared to the rest of the arrays.

The following figures (Figs. 6–8) show the values of MG versus VG for Cases 1, 2 and 4. Case 3 is not included as this case failed to meet the acceptance criteria in terms of the overall statistical indicators as shown in Table 3. The parabola represents the minimum possible value of VG corresponding to a particular MG due to systematic bias. All points must lie either on the parabola or inside. The points close to the parabola indicate systematic errors whereas the ones close to the central axis (MG = 1) indicate dispersion of the results. Points on the left hand side of the central axis indicate a tendency of the simulation results to over-prediction while the opposite tendency occurs for the points on the right hand side. For a perfect agreement between the simulation results and the experimental data, the point should be in the parabola vertex (1,1). In all cases, the results showed a trend of decreasing numerical

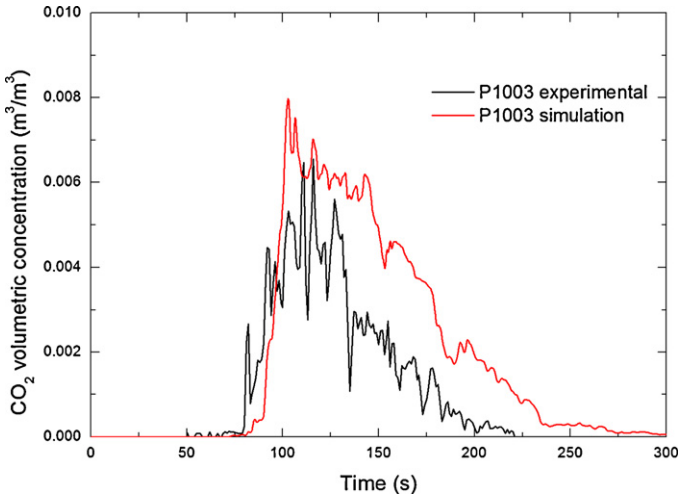

Fig. 5. Comparison of experimental CO_2 concentration readings with simulation at sensor P1003 (release starts at 50 s).

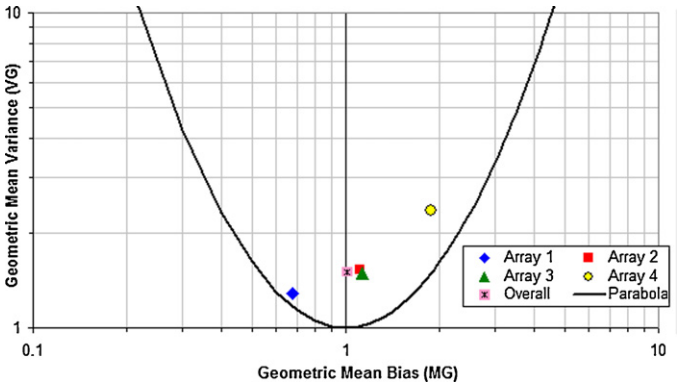

Fig. 6. Plot of geometric mean bias (MG) versus geometric mean variance (VG) for Case 1 (fully resolved obstacles and variable with time wind profile). The maximum experimental concentration in array 4 was 650 ppm which is almost one order of magnitude smaller than the lowest exposure limit.

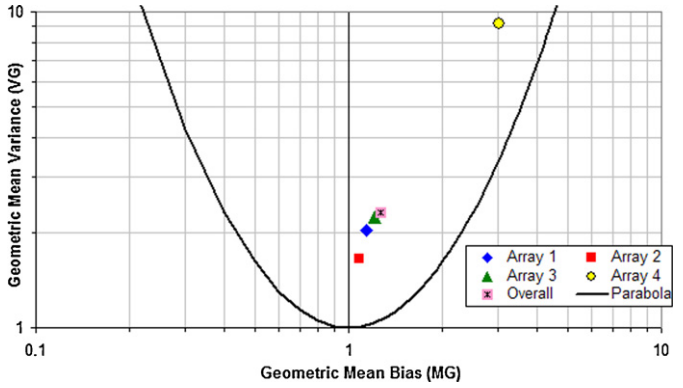

Fig. 7. Plot of geometric mean bias (MG) versus geometric mean variance (VG) for Case 2 (fully resolved obstacles and constant with time wind profile).

accuracy downwind from the source with the results from array 4 performing the worst for all cases as shown by the increasing value of VG. The behavior in the last array (array 4) is partly expected as the maximum observed CO_2 concentration in the array is very low (650 ppm). Values lower than 650 ppm get closer to the limits of the numerical accuracy. Additionally, the mean annual background concentration is currently about 380 ppm for clean air during well-mixed daytime conditions and during the night it can increase by

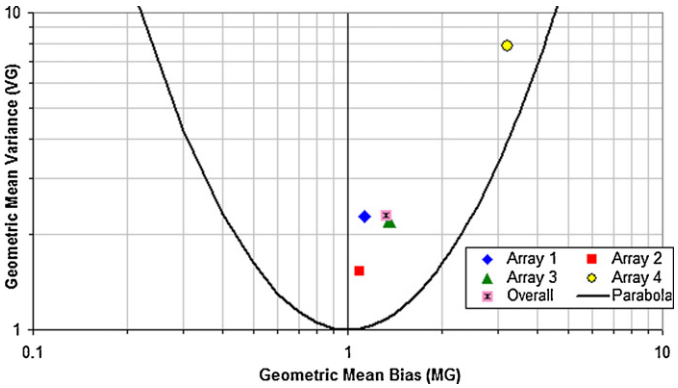

Fig. 8. Plot of geometric mean bias (MG) versus geometric mean variance (VG) for Case 4 (fully resolved ERP obstacles, roughness instead of URA obstacles and constant with time wind profile).

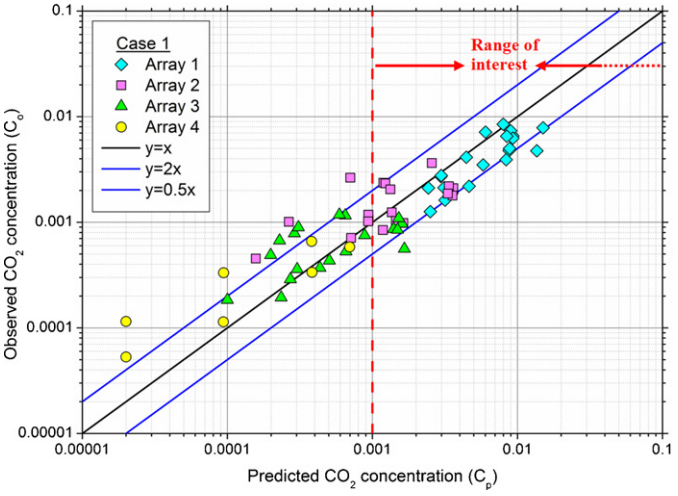

Fig. 9. Scatter plot of observed versus predicted concentrations for Case 1.

100–200 ppm due to biogenic sources [21]. Thus detecting relatively modest changes in CO_2 concentrations above the background level is a quite demanding task. On the other hand, the exposure concentration thresholds range from a value of 100,000 ppm for 1–2 min of exposure time to 5000 ppm for an exposure of 8 h [5,6]. The maximum concentration recorded in the last array (650 ppm) is still one order of magnitude smaller than the lowest threshold of 5000 ppm. Therefore the decreasing accuracy of the code in that range of concentrations should not have a significant impact on a consequence analysis based on the CFD results.

As expected, the results of Case 1 were the ones with the least scatter and bias due to a complete representation of the obstacles in the computational mesh and to a more accurate description of the wind condition in the simulation. However the computational effort for Case 1 was the highest among all cases. The simulations were run on an Intel® Xeon® CPU X5570 @ 2.93 GHz system with 8 CPUs and the HPMPI communication method. The total simulation time for Case 1 was almost 25 days whereas the time was reduced by 2/3 when the constant in time wind profile was used (Case 2 and 3) and was further reduced by almost half when the URA obstacles were substituted by a ground roughness (Case 4).

Figs. 9 and 10 show the scatter plots of observed versus predicted concentrations of the most demanding and the least demanding case in terms of computational effort (Case 1 and 4 respectively). Ideally, in a simulation with results perfectly matching the experimental data, all points should lie on the black line. The two blue lines define an acceptable scatter range corresponding to

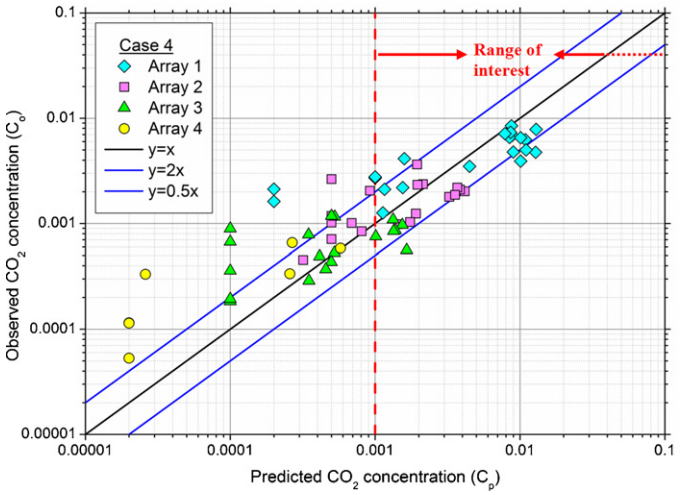

Fig. 10. Scatter plot of observed versus predicted concentrations for Case 4.

a factor of 2 for over and under prediction. As mentioned before, the lowest exposure limit for CO_2 is set to 5000 ppm (0.005 m^3/m^3). Since the main scope of this work was to assess the accuracy of the code and validate its performance for future CO_2 safety studies a reasonable range of concentration of interest can be set higher than 0.001 m^3/m^3. The figures show that generally, the sensors located in the last 2 arrays had the largest scatter whereas their respective concentrations were less than 0.001 m^3/m^3. A comparison between the two figures shows that the added value of the results is not counterbalanced by the high computational effort for the relevant concentration levels (>0.001 m^3/m^3). However, in order to generalize this conclusion, more experimental tests should be simulated and analyzed following a similar approach since in the current work one experimental test was used, which covered a short CO_2 release with a wind velocity profile having a maximum and a minimum not higher than 50% of the average wind velocity (see Fig. 2). Another relevant parameter is the effect of the variation of the direction of the wind. In the present work, this parameter was not investigated since the variation during the experimental test was insignificant.

The 3.65 kg/s CO_2 release rate of the present study is comparable to the one that could be expected from a small leak of a CCS pipeline at high pressure. For example, Mazzoldi et al. [17] calculated a 3.7 kg/s CO_2 release flow rate from a 10 mm leak of a pipeline at 10 MPa pressure. Nevertheless it must be emphasized that although the release flow rate is similar in the two cases, the flow conditions in the vicinity of the leak are different. In a leak of high pressure CO_2, the flow is released at choked conditions. Additionally, if the CO_2 is in a supercritical state the release will involve phase changes. Therefore the release that was simulated in this study can represent the mixing of CO_2 with air and the dispersion of the toxic cloud but it cannot represent the flow conditions in the region close to the leak. The Kit Fox experiments were selected due to the lack of more representative experiments to CCS accidental scenarios in the available scientific literature. Experiments found in the literature involving a high pressure or supercritical CO_2 were aimed at calculating the release conditions at the leak and not the dispersion of the cloud in the far field [18–20]. Also, CO_2 geo-sequestration experiments have been reported recently [21]. These experiments were designed to provide information for monitoring geo-sequestration rather than an accidental case that could pose a direct threat to human life and the environment and thus they involved a slow CO_2 gas release (0.5–1.2 g/s) whereas the furthest measurements were taken 30 m from the source.

The figures below show the extent of contours of CO_2 exposure thresholds at 10 s after the beginning of the release (Fig. 11) and

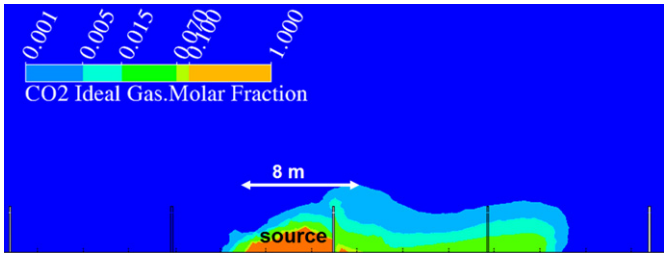

Fig. 11. Contours of CO_2 exposure thresholds at 10 s after the beginning of the release (Case 1). The exposure thresholds are: (a) 8 h Long Term Exposure Limit: 0.005 m^3/m^3, (b) 15 min Short Term Exposure Limit: 0.015 m^3/m^3 and (c) immediately dangerous to human life concentration threshold: 0.07–0.1 m^3/m^3.

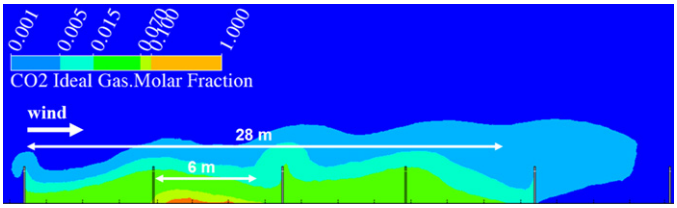

Fig. 12. Contours of CO_2 exposure thresholds at 10 s after the end of the release (Case 1) (release duration: 20 s).

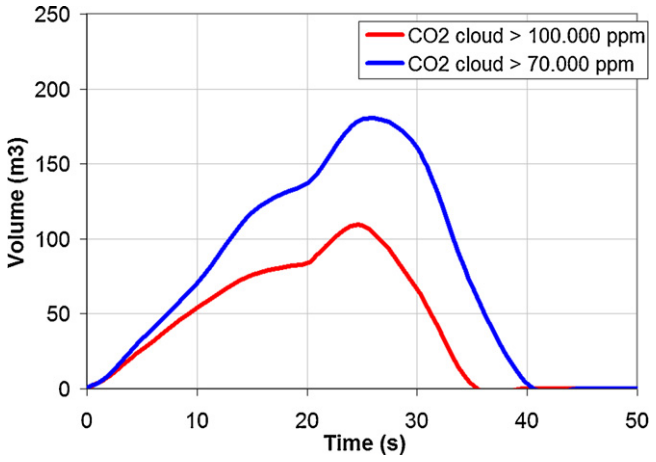

Fig. 13. Time evolution of CO_2 cloud volume with immediately dangerous to life concentrations (Case 1).

at 10 s after the end (Fig. 12) for Case 1. At 10 s after the beginning of the release there is a CO_2 cloud close to the release area that is immediately dangerous to human life (7×10^{-2} to 10^{-1} m^3/m^3). The length of this cloud is approximately 8 m. After 10 s from the end of the release the same cloud has approximately 6 m length whereas the cloud with a CO_2 concentration threshold for 15 min exposure limit (15,000 ppm) is approximately 17 m long in the direction of the wind and 11 m in the opposite direction. It has to be emphasized that the development of the 15,000 ppm cloud is not relevant in this case because its residence time is smaller than the exposure limit (15 min) for that concentration threshold.

The following figure (Fig. 13) shows the time evolution of the CO_2 cloud volume with concentrations greater than 70,000 ppm and 100,000 ppm which are considered as immediately dangerous to human life. These two clouds disappear at approximately 25 s and 15 s from the end of the release respectively. Finally, the simulation showed that after approximately 80–90 s from the end of the release no CO_2 clouds with exposure threshold concentrations were present in the field.

As a last consideration, this validation exercise provides relevant indications on the model accuracy and on the safety margins that should be used in case of application of the code/model to a real accident scenario with conditions similar to those in the selected experiment. If a modeling approach similar to Case 4 (i.e. constant wind profile and a roughness on the mesh representing small obstacles) is applied, then the exposure thresholds should be modified according to the results shown in Table 3. For example, the VG = 2.29 in Case 4 is equivalent to an average ratio between the experimental data and the simulation results equal to 2.48. It is advised to multiply and divide the toxic threshold by roughly 2.5 to arrive at a conservative estimate of the development of the size and position of the toxic cloud.

6. Conclusions

The numerical results of a short CO_2 release from the Kit Fox experiments were compared in a systematic way against data in order to evaluate the accuracy of the CFX 12.1 code. Two parameters were identified from the literature review as among the most influential in modeling large scale gas field experiments; the modeling approach for the description of the wind conditions and the one for representing the presence of obstacles in the computational mesh. It was decided to investigate both of them by simulating 4 cases and comparing the results with the selected experiment. In 3 of the cases both small and big obstacles were fully resolved on the mesh with a variable wind profile, a constant profile and a constant profile with double wind velocity than the averaged in time experimental one. In the last case, the small obstacles were substituted by an appropriate roughness height having a constant wind profile.

The results were evaluated using statistical performance indicators for the ratio of the maximum observed to predicted CO_2 concentrations. The statistical indicators showed that there is a trend of decreasing numerical accuracy with downwind distance from the source with the results of the furthest array (225 m away from the source) performing the worst for all cases. The results of the case with a variable wind profile and fully resolved obstacles had the least scatter and bias. However, the computational effort was the highest among all cases. Bearing in mind that the scope of this work is to evaluate the performance of the code and the different modeling approaches for future CO_2 safety studies, the cases with constant wind and a roughness instead of the small obstacles produced results within the acceptable range as well, for concentration readings higher than 1000 ppm. Finally, the case with double constant wind profile performed the worst and in general did not meet the acceptable criteria of the statistical indicators.

Future work should include numerical simulation with a wide range of weather conditions and duration and direction of the release. As soon as experimental data of release and dispersion of high pressure or supercritical CO_2 become available in the scientific literature, validation of the current CFD models and codes would be continued.

Acknowledgement

The authors would like to thank Dr. J. C. Chang and Dr. S. Hanna for kindly providing the data of the Kit Fox experiments.

References

[1] International Energy Agency (IEA), Energy technology policy division, technology roadmap: carbon capture and storage, 2009, http://www.iea.org/papers/2009/CCS_Roadmap.pdf.
[2] COM, A Technology Roadmap for the Communication on Investing in the Development of Low Carbon Technologies (SET-Plan), 2009.
[3] COM, 13 Final Communication from the Commission to the European Parliament, the Council, the European Economic and Social Committee and the Committee of the Regions, Supporting Early Demonstration of Sustainable Power Generation from Fossil Fuels, 2008.
[4] Directive 2009/31/EC of the European Parliament and of the Council of 23 April 2009 on the geological storage of carbon dioxide.
[5] HSE Guidance EH40/2005, Workplace Exposure Limits, http://www.hse.gov.uk/coshh/table1.pdf.
[6] IPCC, Special Report on Carbon Dioxide Capture and Storage, 2005.
[7] ANSYS, CFX-12.1, Canonsburg Pennsylvania, 2009, http://www.ansys.com.
[8] Western Research Institute, The 1995 Kit Fox Project: Volume I—Experiment description and data processing, Final Report for Task 19, 1998.
[9] S.R. Hanna, J.C. Chang, Use of Kit Fox field data to analyze dense gas dispersion modeling issues, Atmos. Environ. 35 (2001) 2231–2242.
[10] S.R. Hanna, O.R. Hansen, S. Dharmavaram, FLACS CFD air quality model performance evaluation with Kit Fox, MUST, Prairie Grass and EMU observations, Atmos. Environ. 38 (2004) 4675–4687.
[11] A. Mazzoldi, T. Hill, J.J. Colls, CFD and Gaussian atmospheric dispersion models: a comparison for leak from carbon dioxide transportation and storage facilities, Atmos. Environ. 42 (2008) 8046–8054.
[12] Pointwise Inc., Gridgen, Fort Worth, Texas, USA, http://www.pointwise.com/gridgen/.
[13] A. Luketa-Hanlin, R.P. Koopman, D.L. Ermak, On the application of the computational fluid dynamics codes for liquefied natural gas dispersion, J. Hazard. Mater. 140 (2007) 504–517.
[14] J.C. Kaimal, J.J. Finnigan, Atmospheric Boundary Layer Flows—Their Structure and Measurement, Oxford University Press, 1994.
[15] M. Pontiggia, M. Derudi, V. Busini, R. Rota, Hazardous gas dispersion: a CFD model accounting for atmospheric stability classes, J. Hazard. Mater. 171 (2009) 739–747.
[16] J.C. Chang, S.R. Hanna, Technical description and User's guide for the BOOT statistical model evaluation software package, Version 2.0, 2005.
[17] A. Mazzoldi, T. Hill, J.J. Colls, CO_2 transportation for carbon capture and storage: sublimation of carbon dioxide from a dry ice bank, Int. J. Greenhouse Gas Control 2 (2008) 210–218.
[18] B. Gebbeken, R. Eggers, Blowdown of carbon dioxide from initially supercritical conditions, J. Loss Prev. Process Ind. 9 (4) (1996) 285–293.
[19] A. Fredenhagen, R. Eggers, High pressure release of binary mixtures of CO_2 and N_2. Experimental investigation and simulation, Chem. Eng. Sci. 56 (2001) 4879–4885.
[20] G.P. Mignot, M.H. Anderson, M.L. Corradini, Measurement of supercritical CO_2 critical flow: effects of L/D and surface roughness, Nucl. Eng. Des. 239 (2009) 949–955.
[21] Z. Loh, R. Leuning, et al., Testing Lagrangian atmospheric dispersion modelling to monitor CO_2 and CH_4 leakage from geosequestration, Atmos. Environ. 43 (2009) 2602–2611.
[22] J. Blazek, Computational Fluid Dynamics: Principles and Applications, 1st ed., Elsevier, 2001, pp. 316.
[23] J.H. Ferziger, M. Peric, Computational Methods for Fluid Dynamics, 3rd ed., Springer, 2001, pp. 336.